HHS Public Access

Author manuscript

Int J Obes (Lond). Author manuscript; available in PMC 2019 December 22.

Published in final edited form as:

Int J Obes (Lond). 2020 January ; 44(1): 254–266. doi:10.1038/s41366-018-0315-7.

Deletion of translin (*Tsn*) induces robust adiposity and hepatic steatosis without impairing glucose tolerance

Aparna P. Shah[1,*], **Miranda D. Johnson**[2,*], **Xiuping Fu**[1,*], **Gretha J. Boersma**[2,5], **Madhura Shah**[1], **Michael J. Wolfgang**[3,4], **Kellie L. Tamashiro**[2], **Jay M. Baraban**[#,1,2]

[1]Solomon H. Snyder Department of Neuroscience, Johns Hopkins University School of Medicine, Baltimore, MD 21205, USA [2]Department of Psychiatry and Behavioral Sciences, Johns Hopkins University School of Medicine, Baltimore, MD 21205, USA [3]Department of Biological Chemistry, Johns Hopkins University School of Medicine, Baltimore, MD 21205, USA [4]Center for Metabolism and Obesity Research, Johns Hopkins University School of Medicine, Baltimore, MD 21205, USA [5]Present address: GGZ Drenthe Mental Health Institute, Department of Forensic Psychiatry, Assen, The Netherlands

Abstract

Objective: Translin knockout (KO) mice display robust adiposity. Recent studies indicate that translin and its partner protein, trax, regulate the microRNA and ATM kinase signaling pathways, both of which have been implicated in regulating metabolism. In the course of characterizing the metabolic profile of these mice, we found that they display normal glucose tolerance despite their elevated adiposity. Accordingly, we investigated why translin KO mice display this paradoxical phenotype.

Methods: To help distinguish between the metabolic effects of increased adiposity and those of translin deletion per se, we compared three groups: (1) wild-type (WT), (2) translin KO mice on a standard chow diet, and (3) adiposity-matched WT mice that were placed on a high-fat diet until they matched translin KO adiposity levels. All groups were scanned to determine their body composition and tested to evaluate their glucose and insulin tolerance. Plasma, hepatic and adipose tissue samples were collected and used for histological and molecular analyses.

Results: Translin KO mice show normal glucose tolerance whereas adiposity-matched WT mice, placed on a high-fat diet, do not. In addition, translin KO mice display prominent hepatic steatosis that is more severe than that of adiposity-matched WT mice. Unlike adiposity-matched WT mice, translin KO mice display three key features that have been shown to reduce susceptibility to

[#]Corresponding author: Jay M. Baraban, Solomon H. Snyder Department of Neuroscience and Department of Psychiatry and Behavioral Sciences, Johns Hopkins University School of Medicine, 725 N Wolfe Street, Hunterian Room 803, Baltimore, MD 21205, USA, Phone: +1410-955-2499, jay.baraban@gmail.com.

[*]These authors contributed equally to this work

Competing Interests

None of the authors have any competing financial interests in relation to the work described.

Supplementary Information is available at the *International Journal of Obesity*'s website.

insulin resistance: increased accumulation of subcutaneous fat, increased levels of circulating adiponectin and decreased Tnfα expression in hepatic and adipose tissue.

Conclusions: The ability of translin KO mice to retain normal glucose tolerance in the face of marked adipose tissue expansion may be due to the three protective factors noted above. Further studies aimed at defining the molecular bases for this combination of protective phenotypes may yield new approaches to limit the adverse metabolic consequences of obesity.

Introduction

The increasing prevalence of obesity-linked diabetes and its medical consequences has invigorated interest in understanding the pathogenesis of these disorders. Characterization of animal models with elevated adiposity is a top priority as this approach has the potential to yield new insights helpful in combating these metabolic disorders. From this perspective, mice lacking translin, are particularly interesting since they display robust adiposity comparable to that found in MC3R knockout mice [1, 2], yet their metabolic profile has not been characterized.

Studies aimed at defining translin's role in cellular signaling have revealed that it binds to a homologous partner protein, translin associated factor X (trax) to form a microRNA-degrading enzyme [3, 4]. In addition, trax, acting independently of translin, binds to and activates ATM kinase [5]. While this kinase is well-known for its role in DNA repair, it also regulates other cellular processes, including insulin signaling [6]. As translin deletion also causes loss of trax protein expression, dysregulation of either microRNA or ATM signaling pathways might contribute to metabolic phenotypes displayed by translin KO mice.

In preliminary studies characterizing the metabolic profile of translin KO mice, we unexpectedly found that these mice display normal glucose tolerance despite their elevated adiposity on a standard (low-fat) diet. Accordingly, we investigated the basis for this paradoxical phenotype.

Materials and Methods

Animals

A colony of translin KO mice was established at Johns Hopkins University from the line generated in Dr. Kasai's laboratory, which had been backcrossed to C57/BL6 mice for over ten generations [7] and then provided to us by the JCRB Laboratory Animal Resource Bank of the National Institute of Biomedical Innovation. Genotyping was conducted by Transneytx, Inc. (Cordova, TN). Mice were housed in ventilated racks, on a 14-h/10-h light/dark cycle, with standard chow (2018SX Teklad Global, Frederick, MD; unless stated otherwise) and water available *ad libitum*. For the comparative study involving adiposity-matched WT mice, ~16-week-old male WT mice were placed on a 60% high-fat diet (HFD; D12492, Research Diets, New Brunswick, NJ) for 7 weeks (WT-HFD). Age-matched translin KO and WT control (KO-LFD and WT-LFD) groups received a 10% low-fat diet (LFD; D12450J, Research Diets) for the same duration. At start, WT mice were allocated to either -LFD or -HFD groups based on body weights and body composition ensuring that there were no differences between these groups at baseline, before intervention. All

procedures were performed in accordance with the NIH's Guide for the Care and Use of Laboratory Animals and approved by the Johns Hopkins Animal Care and Use Committee.

Body Composition

To determine body composition in live mice, nuclear magnetic resonance imaging (EchoMRI-100, Houston, TX) was performed without anesthesia. To determine distribution of subcutaneous and visceral fat in mice carcasses, an established procedure, described by Clegg et al. [8], was used.

Indirect Calorimetry

Oxygen consumption (VO_2), carbon dioxide production (VCO_2), respiratory exchange ratio (RER), energy expenditure (EE), locomotor activity and food intake for ~8-week-old WT and translin KO mice were determined using indirect calorimetric measurements in an open-flow indirect calorimeter (Oxymax; Columbus Instruments, Columbus, OH). Mice were allowed to acclimate to the metabolic chambers for 48 h. Data for VO_2 and VCO_2 rates, locomotor activity and food intake were collected over the subsequent 72-h period in 18-min intervals, using CLAX software (v5.22). The RER ($=VCO_2/VO_2$) was used to evaluate relative oxidation of fat (RER approaching 0.7) versus carbohydrate (RER approaching 1.0). EE was calculated using the Lusk equation ($EE=(3.815+(1.232*RER)*VO_2$) as outlined by CLAX software. EE and food intake were analyzed by ANCOVA using SigmaPlot 14, as recommended by Tschöp et al. [9]. Data shown here represent two cohorts run at different times. Each cohort had an equal number of WT and translin KO mice. Values for VO2 and VCO2 identified as outliers by Grubb's outlier test were excluded (n = 1/group). Corresponding RER and EE values were also excluded. Food intake data for three animals (n = 2 for WT and 1 for KO) were excluded due to food spillage.

Histological Assessment

5-μm-thick sections of paraffin-embedded liver and epididymal white adipose tissue (eWAT) samples were stained with haematoxylin and eosin (H&E) and imaged using brightfield microscopy (KEYENCE BZ-X700, Itasca, IL). For adipocyte area quantification, images of three random fields within an eWAT section, with well-defined cell boundaries and minimum vasculature or tissue damage, were acquired per animal. Morphometric analysis was performed using Adiposoft (Fiji plug-in; [10]); by an experimenter naive to group assignments. Cells with areas less than 350-μm^2 and those extending beyond the image boundary, were excluded. Percentage frequency distributions were compared using the Friedman test and pairwise comparisons were made by Dunn's post-hoc test.

Glucose Tolerance Test and Insulin Tolerance Test

The intraperitoneal glucose tolerance test (ip-GTT) was performed as previously described [11]. 5- or 10-month old-mice were habituated to the testing room for 1 h, after an overnight fast (~16 h). At 0900 h, baseline glucose levels were measured using handheld glucometers (Freestyle; Abbott, Alameda, CA) via tail nick. Additionally, blood was collected in heparin-coated capillary tubes for analysis of baseline plasma insulin levels. Mice were then injected with glucose (1.5 mg/g, i.p.). Blood glucose level measurements and blood collection for

insulin levels occurred at 15, 30, 45, 60- and 120-min post-glucose injection. Blood was centrifuged at 4°C at 3000 rpm for 20 min to obtain plasma for assessing insulin levels by ELISA (described below). A WT animal from both the 5 and 10-month cohorts died during ip-GTT. All timepoints for these animals were excluded. For the i.p. insulin tolerance test (ip-ITT), mice were fasted for ~5 h and baseline glucose was measured. Mice were then injected with insulin (0.75 mU/g; Humulin R; Lilly, Indianapolis, IN) [12]. Blood glucose levels were measured using handheld glucometers (Freestyle) at 15, 30, 45, 60- and 90-min post-insulin injection.

Measurement of Metabolic Parameters

Blood was collected after an ~6 h fast and processed to obtain plasma. Plasma adiponectin and leptin were measured by ELISA (#EZMADP-60K and EZML-82K, MilliporeSigma, Billerica, MA). Plasma FFAs were measured using fluorometry (#700310, Cayman Chemicals, Ann Arbor, MI). Plasma and liver triglycerides were measured using colorimetry (#10010303, Cayman Chemicals). For samples collected during the ip-GTT, plasma insulin levels were measured by ELISA (#90080, Crystal Chem, Downers Grove, IL).

Real-Time Quantitative RT-PCR

Total RNA was isolated from eWAT and liver using the miRNeasy kit (Qiagen, Hilden, Germany) and assessed for quality (Agilent Bioanalyzer). Samples with RIN < 7 were excluded (n = 1 for WT-HFD eWAT and liver). For gene expression analysis, cDNA was synthesized from 200 ng of total RNA with the High-Capacity cDNA Synthesis kit (Applied Biosystems, Foster City, CA). qRT-PCR was performed using the 2x Fast SYBR Green Master Mix (Applied Biosystems; primer sequences in Supplementary Table 1). miRNAs were reverse-transcribed with specific TaqMan primers (Applied Biosystems), and subsequently measured by real-time PCR with the TaqMan universal PCR master mix and specific TaqMan probes (Applied Biosystems).

Western Blotting

Liver samples were rinsed with PBS and homogenized with RIPA buffer (Cell Signaling Technology, Danvers, MA) containing protease and phosphatase inhibitors (MilliporeSigma, Burlington, MA). Total protein was extracted from eWAT using the Minute Total Protein Extraction Kit for Adipose Tissues (Invent Biotechnologies, Plymouth, MN). Protein concentration was determined using the Pierce BCA Protein Assay Kit (Thermo Fisher Scientific, Waltham, MA). Equal amounts of total protein were separated by an SDS-PAGE gel, transferred to a PVDF membrane and immunoblotted with antibodies: Anti-SIRT1, anti-tubulin (#9475T and #2148, Cell Signaling Technology), anti-translin and anti-trax (generated in our laboratory, [13]) and HSC70 (#PA529221, Thermo Fisher Scientific). Blots were developed with the ECL system. Band intensities were quantified from digital images, by densitometry, using ImageJ.

Microarray Analysis

Total eWAT RNA was biotin-labeled using the FlashTag Biotin HSR RNA Labeling Kit, hybridized to Affymetrix miRNA 4.0 arrays, scanned, and analyzed with Expression

Console software (Thermo Fisher Affymetrix, Santa Clara, CA). The raw CEL file data were extracted using the Partek Genomics Suite 6.6 platform, and the mouse-specific probe sets normalized using the Robust Multi-array Average, RMA, algorithm (Partek, Inc. St Louis, MO). The six knockout samples' log2 signal values were compared in Partek to the six WT samples using a one-way two-tailed ANOVA, yielding the microRNAs' differential expression and statistical significance as fold change and *P*-values, respectively. These data have been deposited as GEO Submission GSE114932.

Statistical Analysis

Data are presented as Mean ± SEM. Statistical significance was evaluated using GraphPad Prism7 and 8 (GraphPad Software, La Jolla, CA). Student's two-tailed *t*-test, *t*-test with Welch's correction, (when groups had unequal variances), or one-way ANOVA (followed by Bonferroni's post-hoc test) were used to compare groups in single-variable experiments. For datasets that did not pass normality tests, the Mann-Whitney U test or the Kruskal-Wallis test (followed by Dunn's post-hoc test) was used. Repeated measures (RM) two-way ANOVA were used to analyze multiple-variable experiments. Pairwise comparisons were made using Bonferroni's post-hoc test. Differences were considered significant at $P<0.05$. Sample sizes are mentioned in the figure legends and represent biological replicates. For the comparative study involving adiposity-matched WT mice, sample sizes were based upon numbers sufficient to establish that the body composition of the WT-HFD group differed significantly from the WT-LFD group but not from the KO-LFD group. Experimenters were blinded to group allocations during data acquisition and analysis.

Results

Effect of Translin Deletion on Body Composition

Consistent with previous reports [1, 2], we found that translin KO mice exhibit a significant increase in body fat compared to age-matched WT mice on standard chow (Figure 1). However, in contrast to previous findings, heterozygous translin KO mice do not display increased adiposity (Supplementary Figure 1). Fat mass (as percent body weight) is elevated (Figure 1A; $P<0.01$ at 7 weeks, 5 and 10 months, different cohorts for each age group); conversely, fat-free mass (as percent body weight) is significantly decreased (Figure 1B; $P<0.01$ at 7 weeks, 5 and 10 months) in translin KO mice compared to age-matched WT mice. Despite their elevated adiposity, KO mice do not weigh more than WT mice. In fact, at 7 weeks, they weigh less than their age-matched controls (Figure 1C; $P=0.0003$). Both subcutaneous and visceral adipose tissue depots (as percent body weight) are elevated in the KO mice as compared to age-matched WT mice (Figure 1D; $P<0.001$). As a percent of total fat mass, translin KO mice have a greater proportion of fat deposited in the subcutaneous depot compared to WT littermates (Figure 1E; $P<0.05$).

Metabolic Characterization of Translin KO Mice

We used indirect calorimetry to measure key parameters of energy expenditure in ~8-week-old translin KO mice. Consistent with their elevated adiposity, they consume less oxygen (VO_2) and produce less carbon dioxide (VCO_2) across both, dark and light cycles (Figure 2A–B; $P<0.01$). Based on their lower VO_2 and VCO_2, translin KO mice have a lower

respiratory exchange ratio (RER), suggesting increased fat oxidation (Figure 2C; $P<0.01$). There are no genotype differences in locomotor activity or core body temperature (Figure 2D and Supplementary Figure 2). ANCOVA conducted for both, EE and food intake, revealed that there is no significant effect of genotype on these metabolic parameters after controlling for fat-free mass (Figure 2E–F).

Impact of Translin Deletion on Glucose Tolerance

Despite their elevated adiposity, ~10-month-old, male translin KO mice display normal glucose tolerance (Figure 3A). Blood glucose and plasma insulin levels are similar between WT and KO mice at baseline and at all timepoints assessed post-glucose load (Figure 3A–B).

Since translin KO mice are glucose tolerant despite elevated adiposity, we sought to determine how translin deletion confers this protective effect by comparing them with adiposity-matched WT mice. Accordingly, we placed age-matched WT animals on a high-fat diet (HFD) and monitored their body composition weekly until they displayed equivalent levels of adiposity with translin KO mice fed a low-fat diet (LFD). In addition, we included a group of WT animals on an LFD in this study, to serve as a control. Prior to being placed on their respective diets, there were no differences in body composition between the WT groups. As expected, KO-LFD mice had elevated adiposity (Figure 3C; %fat mass: $P=0.002$ for WT-LFD vs. KO-LFD, $P<0.0001$ for WT-HFD vs. KO-LFD) and decreased fat-free mass (Figure 3D; $P=0.001$ for WT-LFD vs. KO-LFD, $P<0.0001$ for WT-HFD vs. KO-LFD) relative to both WT groups. By week 6, these two measures were no longer different between KO-LFD and WT-HFD groups; however, both groups differed from the WT-LFD mice (Figure 3C–D; $P<0.05$ for WT-LFD vs. WT-HFD, $P<0.001$ for WT-LFD vs. KO-LFD for %fat mass and %fat-free mass). There were no differences in body weight among the three groups at any timepoint during the study (Figure 3E).

After 6 weeks on their respective diets, fasting blood glucose levels are similar among groups. As found previously, WT-LFD and KO-LFD mice display comparable responses to exogenous glucose load at all timepoints of the GTT. However, adiposity-matched (WT-HFD) mice have elevated blood glucose levels at all timepoints post-injection compared to KO-LFD and WT-LFD mice (Figure 3F; $P<0.05$ at 15, 30, 45, 60 and 120 min). Glucose area under the curve (AUC) is elevated in adiposity-matched (WT-HFD) mice compared to WT-LFD mice ($P=0.004$). As expected, there are no differences in glucose AUC between WT-LFD and KO-LFD groups (Figure 3F (inset)).

Comparison of plasma insulin levels during the GTT among these three groups shows that a glucose load elicits a rapid increase in insulin levels (15-min timepoint compared to baseline) in both, WT-LFD and KO-LFD mice, but not in adiposity-matched (WT-HFD) mice (Figure 3G). Consistent with this observation, the insulin AUC is reduced for the WT-HFD group compared to the KO-LFD group (Figure 3G (inset); $P = 0.04$) Furthermore, plasma insulin levels are significantly higher in the KO-LFD group compared to the WT-LFD groups at the final timepoint (Figure 3G; $P<0.05$ at 120-min). In addition, even though the difference in insulin levels between WT-LFD and KO-LFD groups only reaches significance at the 120-min timepoint, KO-LFD mice show a trend toward higher insulin

levels at all other time points. This may reflect increased insulin secretion by KO-LFD mice to compensate for a mild reduction in their insulin receptor sensitivity. However, KO-LFD (or even WT-HFD) mice do not show severe impairment in insulin sensitivity as assessed by the ITT (Figure 3H).

Characterization of Hepatic Tissue

As elevated adiposity is associated with liver steatosis, we characterized hepatic tissue. Histological analysis revealed prominent accumulation of lipid droplets in the KO-LFD group samples; but only rare, isolated lipid droplets in the WT-LFD and -HFD group samples (Figure 4A). Consistent with the observed steatosis, liver tissue samples from the KO-LFD group have elevated triglyceride levels (Figure 4B; P=0.02 for WT-LFD vs. KO-LFD, P=0.005 for WT-HFD vs KO-LFD). Plasma triglycerides do not differ among the three groups (Figure 4C), whereas plasma free fatty acids are elevated for the KO-LFD group compared to the WT-HFD group (Figure 4D; P=0.004). In addition, liver pyruvate kinase (Lpk) mRNA expression is lower in the WT-HFD group relative to the WT-LFD group (P=0.01); however, Lpk mRNA levels for the KO-LFD group do not differ from either of the other groups. There are no differences in fatty acid synthase (Fas), medium chain acyl-coenzyme A dehydrogenase (Mcad), pyruvate dehydrogenase kinase isozyme (Pdk)4, peroxisome proliferator-activated receptor gamma (Pparγ) and sterol regulatory element-binding protein (Srebp)1c between groups (Figure 4E). Tumor necrosis factor (Tnf)α mRNA levels are decreased in the KO-LFD group (P<0.05 for WT-LFD vs. KO-LFD and for WT-HFD vs. KO-LFD). There are no differences between groups with respect to gene expression for nitric oxide synthase (Nos)2, arginase (Arg)1 and interleukin (Il)10 (Figure 4F).

Recent studies have shown that Sirtuin (SIRT)1 plays an important role in regulating critical metabolic processes in the liver and a decrease in its levels is associated with nonalcoholic fatty liver disease [14]. Therefore, we measured hepatic SIRT1 protein levels. SIRT1 levels are decreased in WT-HFD and KO-LFD groups relative to the WT-LFD group (P=0.01 for WT-LFD vs WT-HFD, P=0.0002 for WT-LFD vs KO-LFD). Hepatic trax protein levels are not altered by diet or degree of adiposity. It is well-established that trax protein, but not trax mRNA, is absent in translin KO mice [15]. Consistent with this finding, trax is not expressed in KO-LFD liver (Figure 4G).

Characterization of Adipose Tissue

Histological analysis revealed that eWAT adipocytes from both, WT-HFD and KO-LFD groups are hypertrophic relative to the WT-LFD group (Figure 5A). This was confirmed quantitatively by comparing the percentage frequency distributions of adipocyte areas, determined by morphometric analysis (P<0.05 for WT-LFD vs. WT-HFD and WT-LFD vs. KO-LFD). Average adipocyte areas correlate with adiposity for all three groups (Figure 5B). Additionally, quantification of translin and trax proteins in eWAT after HFD exposure indicates that their expression does not vary with diet or degree of adiposity. As expected, both translin and trax proteins are absent from KO-LFD eWAT (Figure 5C).

There are no differences in either leptin or adiponectin mRNA levels in eWAT (Figure 6A). Although plasma leptin levels do not differ (Figure 6B), these are highly correlated with

adiposity for all groups, as expected (Supplementary Figure 3A). Plasma adiponectin levels are increased in the KO-LFD group, but not in the adiposity-matched (WT-HFD) group (Figure 6C; P=0.005 for WT-LFD vs KO-LFD, P=0.0003 for WT-HFD vs KO-LFD). Adiponectin levels correlate with adiposity for the WT-HFD group, but not for the WT or KO groups on an LFD (Supplementary Figure 3B). Furthermore, eWAT mRNA levels of Fas (P<0.05) and Pparγ (P<0.05) differ only between the WT-LFD and WT-HFD groups (Figure 6D). There are no differences in adipose triglyceride lipase (Atgl), hormone-sensitive lipase (Hsl), or insulin-regulated glucose transporter (Glut4) among groups. Since adipose tissue inflammation influences glucose metabolism [16], we measured mRNA levels of several inflammation markers, specifically, Tnfα, Nos2, Il10, Arg1 and macrophage galactose-type lectin (Mgl)1 and Mgl2. Interestingly, Tnfα and Nos2 mRNA expression is increased in the adiposity-matched (WT-HFD) group compared to the KO-LFD group (Figure 6E; P<0.05 for WT-HFD vs KO-LFD).

MicroRNAs in Translin KO WAT

Since the translin/trax complex mediates degradation of a subpopulation of microRNAs [3], one possibility is that the metabolic phenotype displayed by translin KO mice reflects blunted degradation of microRNAs targeted by the translin/trax RNase complex. Accordingly, we examined eWAT from translin KO and WT mice for differences in microRNA expression patterns. Microarray analysis revealed differential expression of several microRNAs between the two groups (Figure 6F). qRT-PCR analysis confirmed upregulation of miRs-379–5p (P=0.03), 335–5p (P=0.02), 335–3p (P=0.006) and 1946b (P=0.02) in translin KO mice (Figure 6G). However, microRNAs that appear to be downregulated by microarray analysis do not show differences when assessed by qRT-PCR (Figures 6A and C). Microarray analysis also revealed that pre-miR-335 is significantly overexpressed in translin KO mice. Contrary to our model, this appears to be due to an increase in transcription as primary miR-335 transcript levels, assayed by qRT-PCR, are increased in samples from translin KO mice (Supplementary Figure 4).

Discussion

The major finding of the present study is that translin KO mice have normal glucose tolerance despite a robust increase in adiposity. In contrast, WT mice fed HFD until they achieved comparable adiposity show impaired glucose tolerance, as expected. Further characterization of the metabolic profile of translin KO mice identified three factors that may account for the paradoxical preservation of glucose tolerance in translin KO mice: elevated circulating adiponectin, reduced eWAT Tnfα and Nos2 gene expression compared to the adiposity-matched (WT-HFD) group, and preferential expansion of subcutaneous adipose tissue.

Several studies point to a protective role of adiponectin in preventing the deleterious consequences of obesity. Plasma levels of this adipokine are decreased in mouse models of obesity and in obese patients despite increased fat mass [17, 18]. Furthermore, adiponectin has been shown to maintain “healthy” expansion of adipose tissue by its actions, such as increasing insulin sensitivity and stimulating GLUT4-mediated glucose uptake into skeletal

muscles [19–22]. Consistent with this view, there is an inverse correlation between plasma adiponectin levels and insulin resistance in humans, independent of obesity [23]. Therefore, the maintenance of normal glucose tolerance in translin KO mice may be due, in part, to their elevated adiponectin levels. Of note, recent reports show that translin KO mice have ectopic adipogenesis in bone marrow [24]. Given that bone marrow adipocytes can secrete a disproportionate amount of adiponectin [25], this source may contribute to increased adiponectin levels in these mice.

Another factor that could contribute to preserving normal glucose tolerance is the reduced eWAT Tnfα and Nos2 expression in translin KO mice compared to adiposity-matched WT mice. Furthermore, translin KO mice have lower hepatic Tnfα mRNA expression than either WT-LFD or WT-HFD mice. These proinflammatory cytokines are normally elevated in obesity and are thought to contribute to insulin resistance [18, 26–28]. Therefore, the blunted Tnfα and Nos2 expression in translin KO mice may confer protection against glucose intolerance. Conceivably, reduced Tnfα expression may be secondary to the elevated levels of adiponectin, which is known to have anti-inflammatory effects [29]. Kern et al. [23], report an inverse relationship between plasma adiponectin and adipose-tissue derived Tnfα mRNA expression. Consistent with this finding, rodent studies show that adiponectin treatment suppresses plasma and hepatic levels of this proinflammatory cytokine, whereas adiponectin KO mice have increased adipose tissue Tnfα mRNA and plasma TNFα levels [30, 31].

In addition, translin KO mice display a preferential increase in subcutaneous fat. Expansion of this depot, rather than visceral fat accumulation, is thought to be protective against the development of metabolic syndrome. This pattern of fat deposition was unexpected as accumulation of fat in males generally favors the visceral depot. Further studies investigating how translin deletion elicits this pattern, including gonadal hormone profiling, would be of interest [32–34].

Although our present study has identified several factors that may account for preserving glucose tolerance in translin KO mice, the molecular mechanism underlying their robust adiposity remains unclear. Recent studies show that translin KO mice have altered mesenchymal cell differentiation which could lead to excessive adipogenesis during development [24, 35]. Consistent with this scenario, we found that translin KO mice display increased fat mass and decreased fat-free mass as early as 7 weeks of age.

In addition to prominent expansion of WAT, translin KO mice also display ectopic accumulation of lipids in liver, as evident from the extensive hepatic steatosis and elevated liver triglyceride levels. This pathology is more pronounced in the KO-LFD than in adiposity-matched WT-HFD mice. Since hepatic steatosis is linked to hepatic insulin resistance [36], it is noteworthy that translin KO mice retain normal glucose tolerance. Animal models with liver specific knockdown of SIRT1, a master regulator of hepatic metabolism, show hepatic steatosis [37, 38]. Therefore, it is possible that the prominent steatosis observed in translin KO mice is due to reduced levels of hepatic SIRT1 [39]. However, expression levels of transcription factors downstream of SIRT1, such as Pparγ and Srebp-1c, or of metabolic enzymes regulating glucose or fatty acid metabolism (Fas, Lpk,

Mcad, Pdk4) are not altered in liver samples from translin KO mice indicating that reduced levels of hepatic SIRT1 may not account for this phenotype. Accordingly, further studies are warranted to define the mechanisms mediating hepatic steatosis in these mice.

As recent studies have implicated the microRNA system in regulating energy metabolism and the translin/trax RNase complex mediates degradation of a subpopulation of microRNAs, it is tempting to speculate that defective microRNA degradation present in translin KO mice might contribute to their robust adiposity. To explore this possibility, we assessed the impact of translin deletion on microRNA expression profiles in eWAT. *A priori*, we would expect to see an upregulation of microRNAs that are directly targeted by the translin/trax complex. However, indirect effects of translin deletion and/or adiposity may also elicit up- or down-regulation of other microRNAs. Results of the qRT-PCR studies conducted to validate the microarray findings confirmed increased expression of a small number of microRNAs, namely miRs-335–5p, −335–3p, −379–5p and −1946b. Interestingly, levels of miR-335–5p and miR-379–5p are elevated in adipose tissue harvested from various mouse models of obesity [40–42]. Thus, it is unclear whether these increases are due to the elevated adiposity present in translin KO mice or if they might contribute to increased adiposity. Furthermore, it is important to note that the primary transcript containing miR-335–5p and −3p, pri-miR-335, is also increased in adipose tissue from translin KO mice suggesting that the increase in miR-335 is due to increased transcription rather than impaired degradation.

Previous studies have identified several downstream targets of miR-335–5p that may regulate adipogenesis. For example, miR-335–5p interferes with mesenchymal stem cell differentiation by downregulating Osteoblastogenic runt-related transcription factor 2 (*Runx2*) [43]. Oger et al, [42] report dysregulated expression levels of several previously validated mRNA targets of miR-335–5p in the eWAT from ob/ob mice compared with WT mice, including Tenascin (*Tnc*) and leucine-rich alpha-2-glycoprotein 1 (*Lrg1*) [42]. To the best of our knowledge, there is no direct evidence linking targets of miRs-379–5p to adipogenesis or obesity.

MiRTarBase [44] lists *Il17ra*, the mRNA that encodes interlukin-17 receptor (IL-17R)A, among the experimentally validated targets of miR-1946b. Interestingly, IL-17RA deficiency exacerbates HFD-induced obesity, yet it protects from glucose dysmetabolism [45]. Its ligand, IL-17A, inhibits adipocyte differentiation in mesenchymal stem cells and stimulates pro-inflammatory responses in adipocytes [46]. Taken together, these findings implicate *Il17ra* as an attractive molecular candidate contributing to the metabolic profile displayed by translin KO mice.

In addition to disrupting microRNA signaling, translin deletion could induce adiposity by affecting other aspects of intracellular signaling. First, translin deletion also causes the loss of trax protein [15] which also interacts with other partner proteins to act in a microRNA-independent manner. Recent studies have elegantly demonstrated that trax binds to and activates ATM kinase. In addition to its well-known role in mediating DNA repair, this kinase also plays a prominent role in regulating insulin signaling [6]. Thus, adiposity displayed by translin KO mice might reflect dysregulation of ATM signaling pathways [5,

47]. Second, the translin/trax complex has been shown to bind to the glucose response element of the LPK gene in rat liver extracts and cultured hepatocytes [48, 49], so it may regulate LPK transcription in a microRNA-independent fashion. Thus, both microRNA-dependent and –independent mechanisms need to be considered in designing future studies investigating the molecular mechanisms mediating the metabolic phenotypes induced by translin deletion.

The ability to assess the impact of cell-type selective and inducible deletion of translin using conditional translin KO mice will be valuable for guiding future studies aimed at deciphering how translin deletion causes robust adiposity and hepatic steatosis yet retains normal glucose tolerance.

Supplementary Material

Refer to Web version on PubMed Central for supplementary material.

Acknowledgements

APS, MDJ, and XF contributed equally to this work. APS, MDJ, XF and GJB performed the research. APS, MDJ, XF, GJB, and MS analyzed the data. APS, MDJ, XF, GJB, MJW, KLT, and JMB designed the experiments. APS, MDJ, XF, KLT and JMB drafted the manuscript. GJB and MJW helped revise the manuscript. APS, MDJ, XF, GJB, and KLT, and JMB are the guarantors of this work and, as such, had full access to all the data in the study and take responsibility for the integrity of the data and the accuracy of the data analysis.

The authors thank Dr. Timothy H. Moran (Johns Hopkins University) for reviewing the manuscript and Dr. Andrew Wolfe for assistance with the indirect calorimetric measurements. We thank Ginny Miller, Zachary Cordner, Seva Khambadkone and Leonard Marque for their technical assistance. We also thank Conovor Talbot Jr. (the Johns Hopkins Deep Sequencing and Microarray Core Facility) for the microarray analyses, Michele Pucak (the Johns Hopkins Department of Neuroscience Multiphoton Imaging Core), and Nadine Forbes-McBean (the Johns Hopkins Phenotyping Core). Histological procedures were performed by The Johns Hopkins Medical Institutions Reference Histology Laboratory. This work was supported by an NIH/NIDA grant, DA00266 and NINDS grant NS050274.

References

[1]. Brommage R, Desai U, Revelli JP, Donoviel DB, Fontenot GK, Dacosta CM, et al. High-throughput screening of mouse knockout lines identifies true lean and obese phenotypes. Obesity (Silver Spring). 2008;16:2362–7. [PubMed: 18719666]

[2]. Chennathukuzhi V, Stein JM, Abel T, Donlon S, Yang S, Miller JP, et al. Mice deficient for testis-brain RNA-binding protein exhibit a coordinate loss of TRAX, reduced fertility, altered gene expression in the brain, and behavioral changes. Mol Cell Biol. 2003;23:6419–34. [PubMed: 12944470]

[3]. Asada K, Canestrari E, Fu X, Li Z, Makowski E, Wu YC, et al. Rescuing dicer defects via inhibition of an anti-dicing nuclease. Cell Rep. 2014;9:1471–81. [PubMed: 25457613]

[4]. Baraban JM, Shah A, Fu X. Multiple Pathways Mediate MicroRNA Degradation: Focus on the Translin/Trax RNase Complex. Adv Pharmacol 2018;82:1–20. [PubMed: 29413516]

[5]. Wang JY, Chen SY, Sun CN, Chien T, Chern Y. A central role of TRAX in the ATM-mediated DNA repair. Oncogene. 2016;35:1657–70. [PubMed: 26096928]

[6]. Yang DQ, Kastan MB. Participation of ATM in insulin signalling through phosphorylation of eIF-4E-binding protein 1. Nat Cell Biol. 2000;2:893–8. [PubMed: 11146653]

[7]. Fukuda Y, Ishida R, Aoki K, Nakahara K, Takashi T, Mochida K, et al. Contribution of Translin to hematopoietic regeneration after sublethal ionizing irradiation. Biol Pharm Bull. 2008;31:207–11. [PubMed: 18239274]

[8]. Clegg DJ, Brown LM, Woods SC, Benoit SC. Gonadal hormones determine sensitivity to central leptin and insulin. Diabetes. 2006;55:978–87. [PubMed: 16567519]

[9]. Tschop MH, Speakman JR, Arch JR, Auwerx J, Bruning JC, Chan L, et al. A guide to analysis of mouse energy metabolism. Nat Methods. 2011;9:57–63. [PubMed: 22205519]

[10]. Galarraga M, Campion J, Munoz-Barrutia A, Boque N, Moreno H, Martinez JA, et al. Adiposoft: automated software for the analysis of white adipose tissue cellularity in histological sections. J Lipid Res. 2012;53:2791–6. [PubMed: 22993232]

[11]. Scott KA, Yamazaki Y, Yamamoto M, Lin Y, Melhorn SJ, Krause EG, et al. Glucose parameters are altered in mouse offspring produced by assisted reproductive technologies and somatic cell nuclear transfer. Biol Reprod. 2010;83:220–7. [PubMed: 20445127]

[12]. Kayser BD, Goran MI, Bouret SG. Perinatal overnutrition exacerbates adipose tissue inflammation caused by high-fat feeding in C57BL/6J mice. PLoS One. 2015;10:e0121954. [PubMed: 25835281]

[13]. Finkenstadt PM, Kang WS, Jeon M, Taira E, Tang W, Baraban JM. Somatodendritic localization of Translin, a component of the Translin/Trax RNA binding complex. J Neurochem. 2000;75:1754–62. [PubMed: 10987859]

[14]. Colak Y, Ozturk O, Senates E, Tuncer I, Yorulmaz E, Adali G, et al. SIRT1 as a potential therapeutic target for treatment of nonalcoholic fatty liver disease. Med Sci Monit. 2011;17:HY5–9. [PubMed: 21525818]

[15]. Li Z, Wu Y, Baraban JM. The Translin/Trax RNA binding complex: clues to function in the nervous system. Biochim Biophys Acta. 2008;1779:479–85. [PubMed: 18424275]

[16]. Kammoun HL, Kraakman MJ, Febbraio MA. Adipose tissue inflammation in glucose metabolism. Rev Endocr Metab Disord. 2014;15:31–44. [PubMed: 24048715]

[17]. Arita Y, Kihara S, Ouchi N, Takahashi M, Maeda K, Miyagawa J, et al. Paradoxical decrease of an adipose-specific protein, adiponectin, in obesity. Biochem Biophys Res Commun. 1999;257:79–83. [PubMed: 10092513]

[18]. Makki K, Froguel P, Wolowczuk I. Adipose tissue in obesity-related inflammation and insulin resistance: cells, cytokines, and chemokines. ISRN Inflamm 2013;2013:139239. [PubMed: 24455420]

[19]. Asterholm IW, Scherer PE. Enhanced metabolic flexibility associated with elevated adiponectin levels. Am J Pathol. 2010;176:1364–76. [PubMed: 20093494]

[20]. Berg AH, Combs TP, Du X, Brownlee M, Scherer PE. The adipocyte-secreted protein Acrp30 enhances hepatic insulin action. Nat Med. 2001;7:947–53. [PubMed: 11479628]

[21]. Tomas E, Tsao TS, Saha AK, Murrey HE, Zhang Cc C, Itani SI, et al. Enhanced muscle fat oxidation and glucose transport by ACRP30 globular domain: acetyl-CoA carboxylase inhibition and AMP-activated protein kinase activation. Proc Natl Acad Sci U S A. 2002;99:16309–13. [PubMed: 12456889]

[22]. Yamauchi T, Kamon J, Waki H, Terauchi Y, Kubota N, Hara K, et al. The fat-derived hormone adiponectin reverses insulin resistance associated with both lipoatrophy and obesity. Nat Med. 2001;7:941–6. [PubMed: 11479627]

[23]. Kern PA, Di Gregorio GB, Lu T, Rassouli N, Ranganathan G. Adiponectin expression from human adipose tissue: relation to obesity, insulin resistance, and tumor necrosis factor-alpha expression. Diabetes. 2003;52:1779–85. [PubMed: 12829646]

[24]. Kasai M, Ishida R, Nakahara K, Okumura K, Aoki K. Mesenchymal cell differentiation and diseases: involvement of translin/TRAX complexes and associated proteins. Ann N Y Acad Sci. 2018.

[25]. Li Z, Hardij J, Bagchi DP, Scheller EL, MacDougald OA. Development, regulation, metabolism and function of bone marrow adipose tissues. Bone. 2018;110:134–40. [PubMed: 29343445]

[26]. Hotamisligil GS, Shargill NS, Spiegelman BM. Adipose expression of tumor necrosis factor-alpha: direct role in obesity-linked insulin resistance. Science. 1993;259:87–91. [PubMed: 7678183]

[27]. Lumeng CN, Bodzin JL, Saltiel AR. Obesity induces a phenotypic switch in adipose tissue macrophage polarization. J Clin Invest. 2007;117:175–84. [PubMed: 17200717]

[28]. Lumeng CN, Deyoung SM, Bodzin JL, Saltiel AR. Increased inflammatory properties of adipose tissue macrophages recruited during diet-induced obesity. Diabetes. 2007;56:16–23. [PubMed: 17192460]

[29]. Ouchi N, Walsh K. A novel role for adiponectin in the regulation of inflammation. Arterioscler Thromb Vasc Biol. 2008;28:1219–21. [PubMed: 18565846]

[30]. Maeda N, Shimomura I, Kishida K, Nishizawa H, Matsuda M, Nagaretani H, et al. Diet-induced insulin resistance in mice lacking adiponectin/ACRP30. Nat Med. 2002;8:731–7. [PubMed: 12068289]

[31]. Xu A, Wang Y, Keshaw H, Xu LY, Lam KS, Cooper GJ. The fat-derived hormone adiponectin alleviates alcoholic and nonalcoholic fatty liver diseases in mice. J Clin Invest. 2003;112:91–100. [PubMed: 12840063]

[32]. Clegg DJ, Riedy CA, Smith KA, Benoit SC, Woods SC. Differential sensitivity to central leptin and insulin in male and female rats. Diabetes. 2003;52:682–7. [PubMed: 12606509]

[33]. Karastergiou K, Fried SK. Cellular Mechanisms Driving Sex Differences in Adipose Tissue Biology and Body Shape in Humans and Mouse Models. Adv Exp Med Biol. 2017;1043:29–51. [PubMed: 29224089]

[34]. Palmer BF, Clegg DJ. The sexual dimorphism of obesity. Mol Cell Endocrinol. 2015;402:113–9. [PubMed: 25578600]

[35]. Ikeuchi Y, Imanishi A, Sudo K, Fukunaga T, Yokoi A, Matsubara L, et al. Translin modulates mesenchymal cell proliferation and differentiation in mice. Biochem Biophys Res Commun. 2018;504:115–22. [PubMed: 30172368]

[36]. Perry RJ, Samuel VT, Petersen KF, Shulman GI. The role of hepatic lipids in hepatic insulin resistance and type 2 diabetes. Nature. 2014;510:84–91. [PubMed: 24899308]

[37]. Ding RB, Bao J, Deng CX. Emerging roles of SIRT1 in fatty liver diseases. Int J Biol Sci. 2017;13:852–67. [PubMed: 28808418]

[38]. Schug TT, Li X. Sirtuin 1 in lipid metabolism and obesity. Ann Med. 2011;43:198–211. [PubMed: 21345154]

[39]. Kemper JK, Choi SE, Kim DH. Sirtuin 1 deacetylase: a key regulator of hepatic lipid metabolism. Vitam Horm. 2013;91:385–404. [PubMed: 23374725]

[40]. Chartoumpekis DV, Zaravinos A, Ziros PG, Iskrenova RP, Psyrogiannis AI, Kyriazopoulou VE, et al. Differential expression of microRNAs in adipose tissue after long-term high-fat diet-induced obesity in mice. PLoS One. 2012;7:e34872. [PubMed: 22496873]

[41]. Nakanishi N, Nakagawa Y, Tokushige N, Aoki N, Matsuzaka T, Ishii K, et al. The up-regulation of microRNA-335 is associated with lipid metabolism in liver and white adipose tissue of genetically obese mice. Biochem Biophys Res Commun. 2009;385:492–6. [PubMed: 19460359]

[42]. Oger F, Gheeraert C, Mogilenko D, Benomar Y, Molendi-Coste O, Bouchaert E, et al. Cell-specific dysregulation of microRNA expression in obese white adipose tissue. J Clin Endocrinol Metab. 2014;99:2821–33. [PubMed: 24758184]

[43]. Tome M, Lopez-Romero P, Albo C, Sepulveda JC, Fernandez-Gutierrez B, Dopazo A, et al. miR-335 orchestrates cell proliferation, migration and differentiation in human mesenchymal stem cells. Cell Death Differ. 2011;18:985–95. [PubMed: 21164520]

[44]. Chou CH, Shrestha S, Yang CD, Chang NW, Lin YL, Liao KW, et al. miRTarBase update 2018: a resource for experimentally validated microRNA-target interactions. Nucleic Acids Res. 2018;46:D296–D302. [PubMed: 29126174]

[45]. Harley IT, Stankiewicz TE, Giles DA, Softic S, Flick LM, Cappelletti M, et al. IL-17 signaling accelerates the progression of nonalcoholic fatty liver disease in mice. Hepatology. 2014;59:1830–9. [PubMed: 24115079]

[46]. Shin JH, Shin DW, Noh M. Interleukin-17A inhibits adipocyte differentiation in human mesenchymal stem cells and regulates pro-inflammatory responses in adipocytes. Biochem Pharmacol. 2009;77:1835–44. [PubMed: 19428338]

[47]. Chern Y, Chien T, Fu X, Shah AP, Abel T, Baraban JM. Trax: A versatile signaling protein plays key roles in synaptic plasticity and DNA repair. Neurobiol Learn Mem. 2018.

[48]. Hasegawa J, Osatomi K, Wu RF, Uyeda K. A novel factor binding to the glucose response elements of liver pyruvate kinase and fatty acid synthase genes. J Biol Chem. 1999;274:1100–7. [PubMed: 9873057]

[49]. Wu RF, Osatomi K, Terada LS, Uyeda K. Identification of Translin/Trax complex as a glucose response element binding protein in liver. Biochim Biophys Acta. 2003;1624:29–35. [PubMed: 14642810]

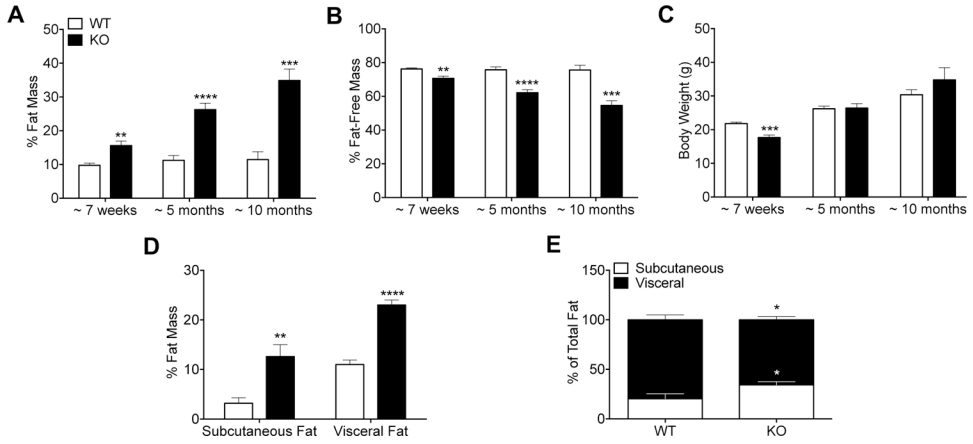

Figure 1: Male translin KO mice on a standard chow diet display elevated adiposity without an increase in body weight.

A: Fat mass (as percent body weight; $t_{(14)} = 4.05$, $P = 0.0012$ at 7 weeks, $t_{(20)} = 6.41$, $P < 0.0001$ at 5 months and $t_{(8)} = 5.74$, $P = 0.0004$ at 10 months) , *B*: Fat-free mass (as percent body weight; $t_{(14)} = 3.87$, $P = 0.0017$ at 7 weeks, $t_{(20)} = 5.57$, $P < 0.0001$ at 5 months and $t_{(8)} = 5.33$, $P = 0.0007$ at 10 months), and *C*: Body weight (in g; $t_{(14)} = 4.82$, $P = 0.0003$ at 7 weeks), for WT and translin KO mice at 7 weeks (n = 8/group), 5 months (n = 11/group) and 10 months (n = 5/group). *D*: Fat mass (as percent of carcass weight; $t_{(8)} = 3.54$, $P = 0.0077$ for subcutaneous and $t_{(8)} = 8.87$, $P < 0.00001$ for visceral adipose tissue) and *E*: Depot-specific proportion of fat mass (as percent of total fat mass; $t_{(8)} = 2.33$, $P = 0.0485$ for subcutaneous and visceral adipose tissue) in 10-month-old WT and translin KO mice (n = 5/group). Data are expressed as Mean ± SEM. $^{**}P \leq 0.01$, $^{***}P \leq 0.001$, $^{****}P \leq 0.0001$ according to Student's *t*-test; (white bars = WT; black bars = translin KO).

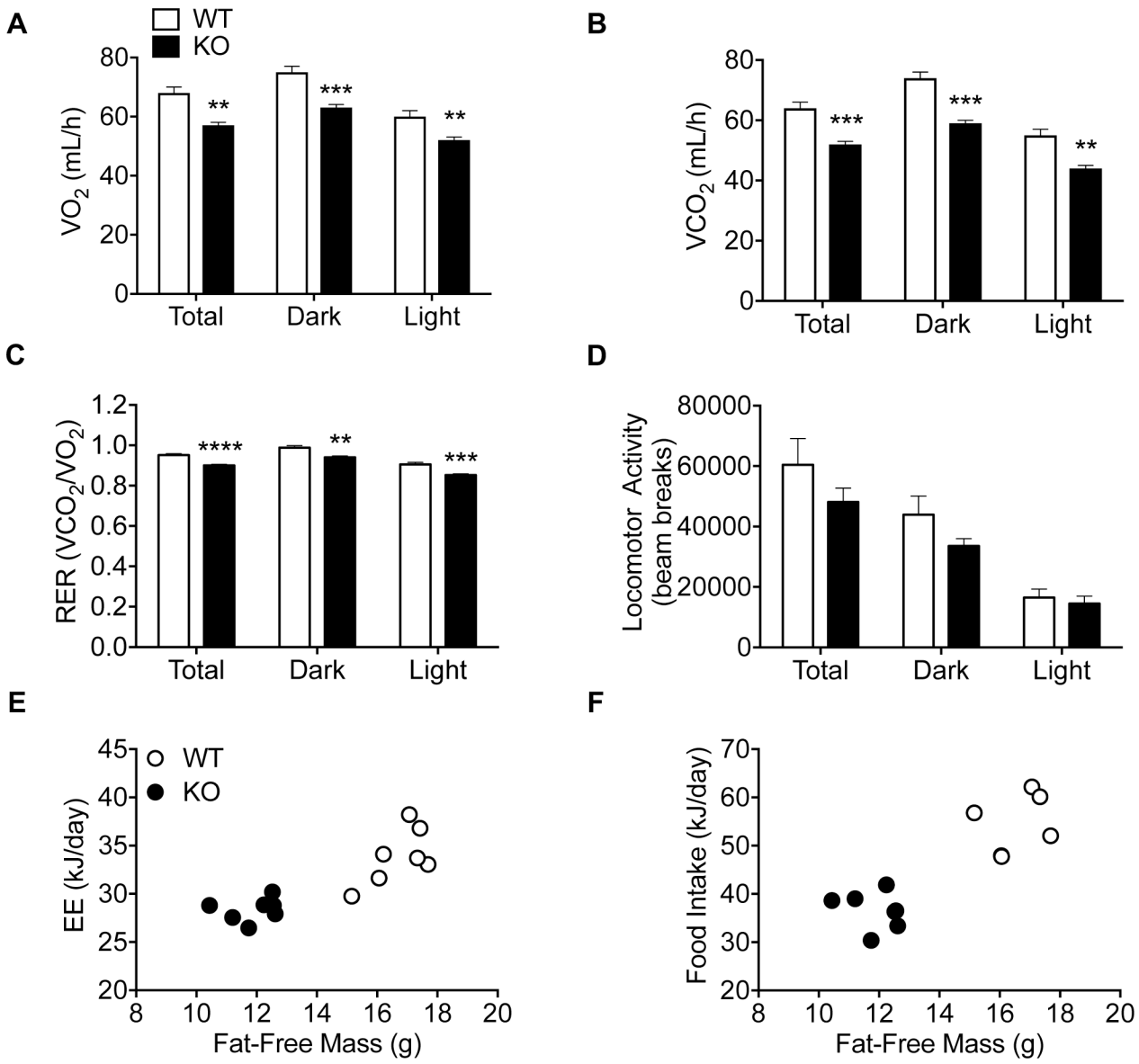

Figure 2: Metabolic characterization of 8-week-old translin KO mice.

A: VO_2, (in mL/h; $t_{(12)} = 4.43$, $P = 0.0023$ for average daily, $t_{(12)} = 5.29$, $P = 0.0009$ for average dark cycle, $t_{(12)} = 3.34$, $P = 0.006$ for average light cycle), *B*: VCO_2, (in mL/h; $t_{(12)} = 5.68$, $P = 0.0005$ for average daily, $t_{(12)} = 6.70$, $P = 0.0002$ for average dark cycle, $t_{(12)} = 3.79$, $P = 0.003$ for average light cycle), *C*: Respiratory exchange ratio (RER=VCO_2/VO_2, ($t_{(12)} = 5.92$, $P < 0.0001$ for average daily, $t_{(12)} = 3.86$, $P = 0.002$ for average dark cycle, $t_{(12)} = 4.56$, $P = 0.0007$ for average light cycle), *D*: Locomotor activity (in number of beam breaks), *E*: Energy expenditure (EE), (in kJ/day) and *F*: Food intake, (in kJ/day) in metabolic chambers across the light and dark cycles vs. Fat-free mass (in g). n = 7/group for VO2, VCO2, RER and EE; n = 8/group for locomotor activity; n = 6 and 7 for the WT and KO groups, respectively, for food intake. Data are expressed as Mean ± SEM.*$P < 0.05$, **$P \leq 0.01$ ***$P \leq 0.001$, and ****$P \leq 0.0001$. Statistical significance was assessed by Student's *t*-test for A-D and ANCOVA for E-F; (white bar/circle = WT; black bar/circle = translin KO).

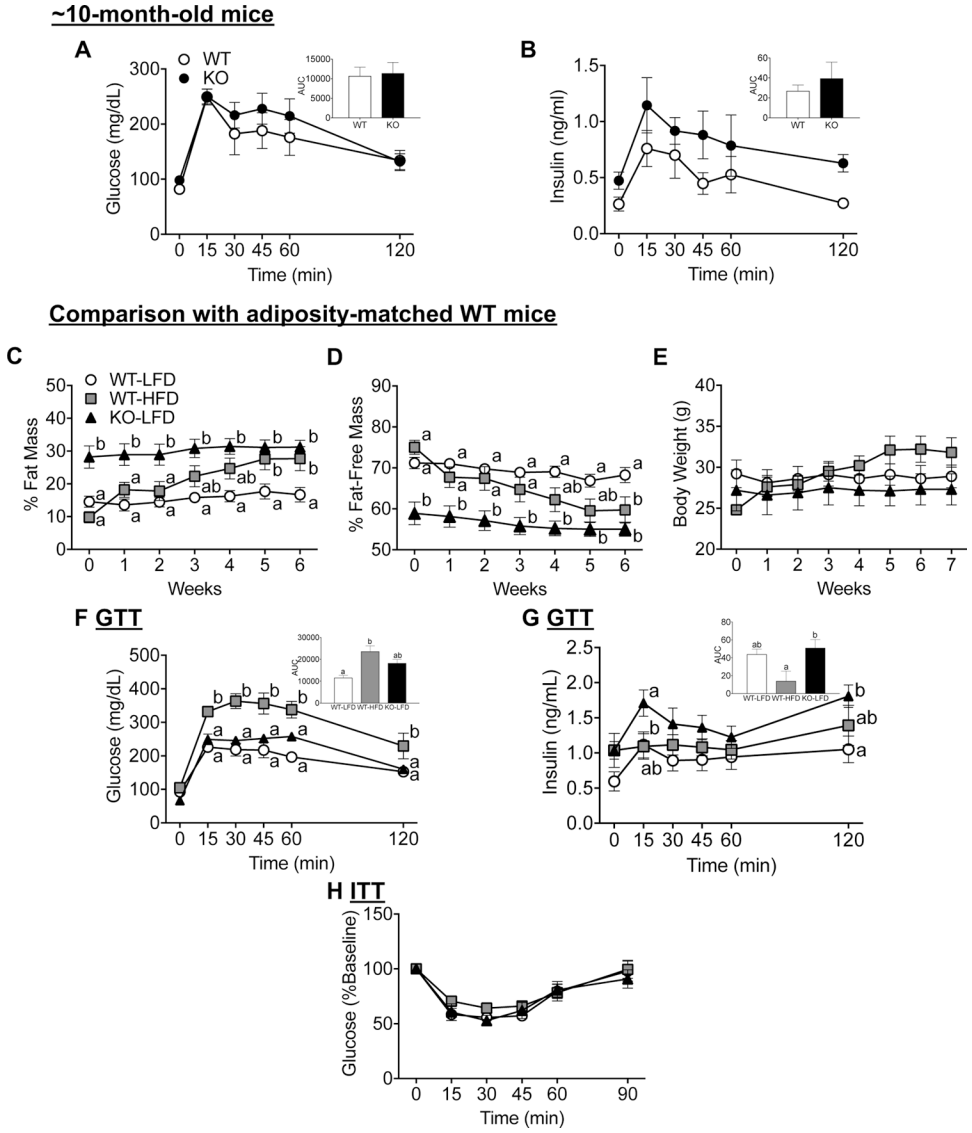

Figure 3: Translin KO mice are glucose tolerant.

~10-month-old mice *A:* Blood glucose (in mg/dL) during ip-GTT (1.5 mg/g glucose), two-way RM ANOVA showed main effects of time ($F_{(5,35)}$ = 15.97, P < 0.00001). *A (inset):* Glucose area under the curve (AUC). *B:* Plasma insulin levels during ip-GTT, two-way RM ANOVA showed main effects of time ($F_{(5,35)}$ = 6.32, P = 0.0003). *B (inset):* Insulin AUC. n = 4–5/group; (white bars/circles = WT; black bars/circles = translin KO). Comparison with age- and adiposity-matched WT mice (~5 months old) *C:* Body fat (as percent body weight), two-way RM ANOVA showed significant group x time interaction ($F_{(12,84)}$ = 15.90, P < 0.0001) and main effects of time ($F_{(6,84)}$ = 43.82, P < 0.0001) and group ($F_{(2,14)}$ = 7.90, P = 0.0051) *D*: Fat-free mass (as percent body weight) two-way RM ANOVA showed significant group x time interaction ($F_{(12,84)}$ = 12.50, P < 0.0001) and main effects of time ($F_{(6,84)}$ = 51.30 P < 0.0001) and group ($F_{(2,14)}$ = 8.98, P = 0.0031) and *E:* Body weight (in g), two-way RM ANOVA showed significant group x time interaction ($F_{(14,98)}$ = 13.71, P < 0.0001) and a main effect of time ($F_{(7,98)}$ = 15.08, P < 0.0001) assessed weekly for WT and translin

KO mice on a low-fat diet (LFD) and WT mice on a high-fat diet (HFD). *F:* Blood glucose (in mg/dL), two-way RM ANOVA showed significant group x time interaction ($F_{(10,70)}$ = 4.42, P < 0.0001) and main effects of time ($F_{(5,70)}$ = 110.90, P < 0.0001) and group ($F_{(2,14)}$ = 13.54, P = 0.0005). *F (inset):* Glucose area under the curve, one-way ANOVA ($F_{(2,14)}$ = 8.04, P = 0.0047). *G:* Plasma insulin levels (in ng/mL) during an ip-GTT (1.5 mg/g glucose), two-way RM ANOVA showed significant group x time interaction ($F_{(10,70)}$ = 2.92, P = 0.0041) and main effects of time ($F_{(5,70)}$ = 18.14, P < 0.0001). *G (inset):* Insulin area under the curve, one-way ANOVA ($F_{(2,14)}$ = 4.43, P = 0.0324). *H:* Blood glucose (in mg/dL) during an i.p. insulin tolerance test (0.75 mU/g insulin), two-way RM ANOVA showed main effects of time ($F_{(4,56)}$ = 34.26, P < 0.0001). n = 5, 6 and 6 for the three groups, respectively. Data are expressed as Mean ± SEM. Different letters indicate statistically significant differences (P < 0.05); (white circles/bars = WT-LFD; grey squares/bars = WT-HFD; black triangles/bars = KO-LFD).

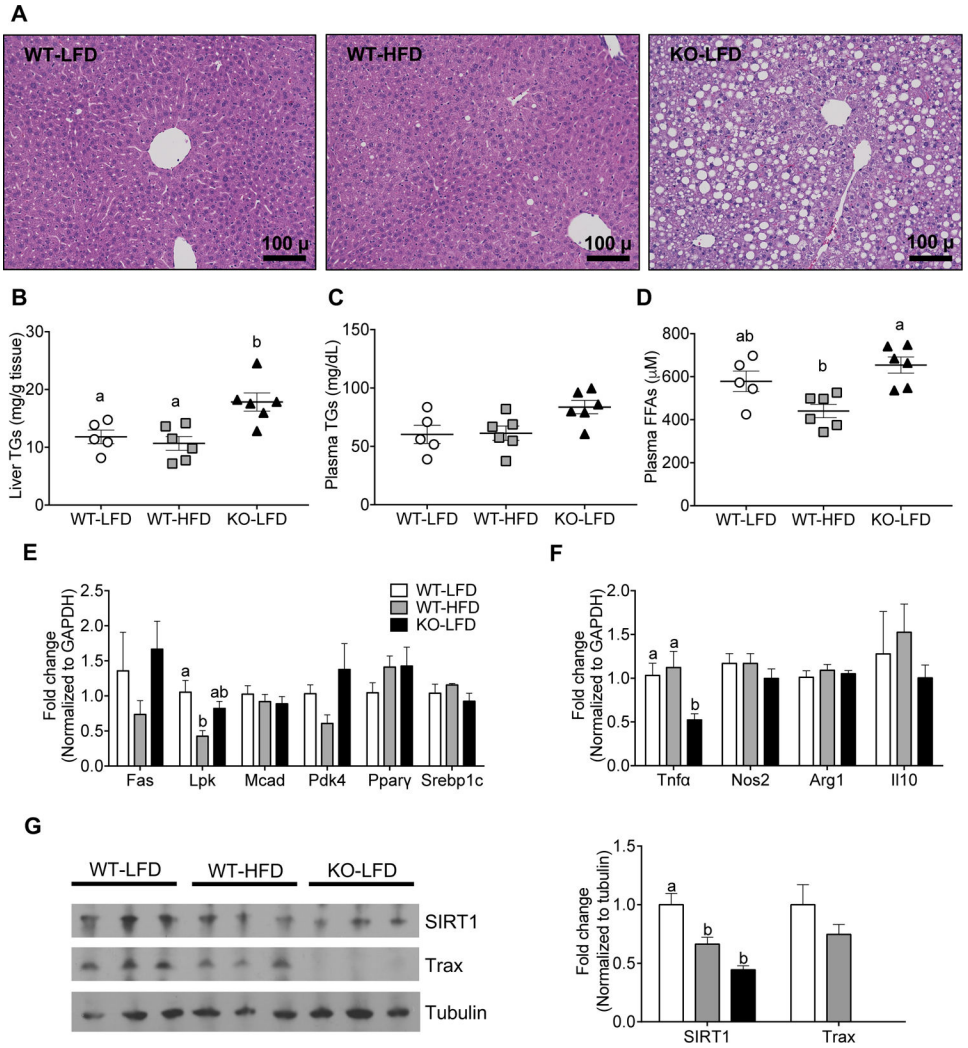

Figure 4: Characterization of hepatic tissue from adult WT and translin KO mice on a low-fat diet (LFD) as well as WT mice on a high-fat diet (HFD) for 7 weeks.

A: Representative images of H&E stained liver sections. Scale bars, 100µ. *B:* Liver TGs (in mg/g tissue), one-way ANOVA ($F_{(2,14)}$ = 8.53, P = 0.0038), *C:* Plasma triglycerides (TGs; in mg/dL), one-way ANOVA ($F_{(2,14)}$ = 4.26, P = 0.036), *D:* Plasma free fatty acids (FFAs; in µM), one-way ANOVA ($F_{(2,14)}$ = 8.43, P = 0.004) . *E:* Relative mRNA levels of Fatty acid synthase (Fas), Liver pyruvate kinase (Lpk), one-way ANOVA ($F_{(2,13)}$ = 6.57 , P = 0.0107), Medium chain acyl-coA dehydrogenase (Mcad), Pyruvate dehydrogenase kinase (Pdk)4, Peroxisome proliferator-activated receptor (Ppar)γ and Sterol regulatory element-binding protein (Srebp)1c normalized to GAPDH. *F:* Relative mRNA levels of inflammation markers - tumor necrosis factor (Tnf)α, one-way ANOVA ($F_{(2,13)}$ = 6.27, P = 0.0124), nitric oxide synthase (Nos)2, arginase (Arg)1 and interleukin (Il)10, normalized to GAPDH. n = 5, 5 and 6 for the three groups, respectively. *G:* Representative bands for SIRT1, one-way ANOVA ($F_{(2,13)}$ = 16.55, P = 0.0003), translin and trax protein in liver tissue (left) and their quantification normalized to tubulin (right). n = 5, 6 and 6 for the three groups, respectively. Data are expressed as Mean ± SEM. Statistical significance was assessed by one-way ANOVA followed by Bonferroni's post-hoc analysis. Different letters indicate statistically

significant differences ($P < 0.05$); (white circles/bars = WT-LFD; grey squares/bars = WT-HFD; black triangles/bars = KO-LFD).

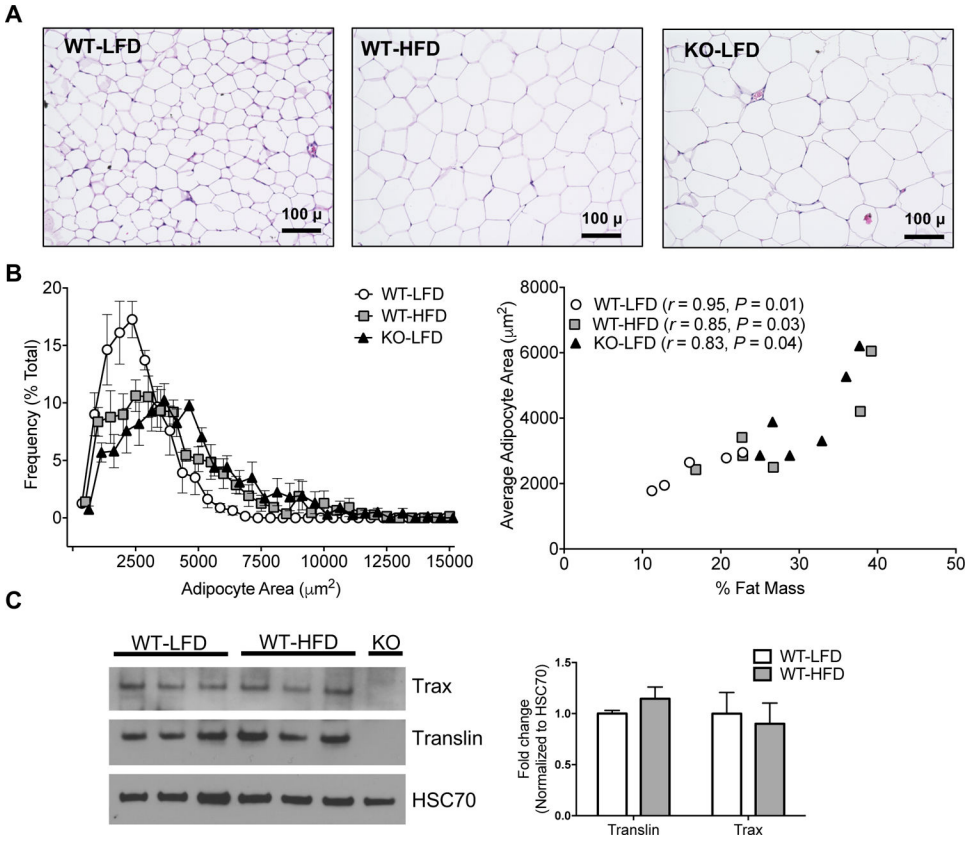

Figure 5: Characterization of adipose tissue.

A: Representative images of H&E stained eWAT. Scale bars, 100µ. *B:* Percentage frequency distribution of adipocyte area (left), Friedman test showed a significant difference between the distributions ($P = 0.0042$) and correlation between %fat mass and average adipocyte area (in µm^2) for WT-LFD ($r = 0.95$, $P = 0.0139$), WT-HFD ($r = 0.85$, $P = 0.0317$) and KO-LFD ($r = 0.83$, $P = 0.0415$) (right). *C:* Representative bands for trax and translin protein in eWAT (left) and their quantification normalized to heat shock cognate 71 kDa (Hsc70) (right). n = 5, 6 and 6 for the three groups, respectively. Data are expressed as Mean ± SEM. Statistical significance was assessed by Student's *t*-test, ordinary or Friedman's test followed by Dunn's post-hoc analysis; (white circles/bars = WT-LFD; grey squares/bars = WT-HFD; black triangles = KO-LFD).

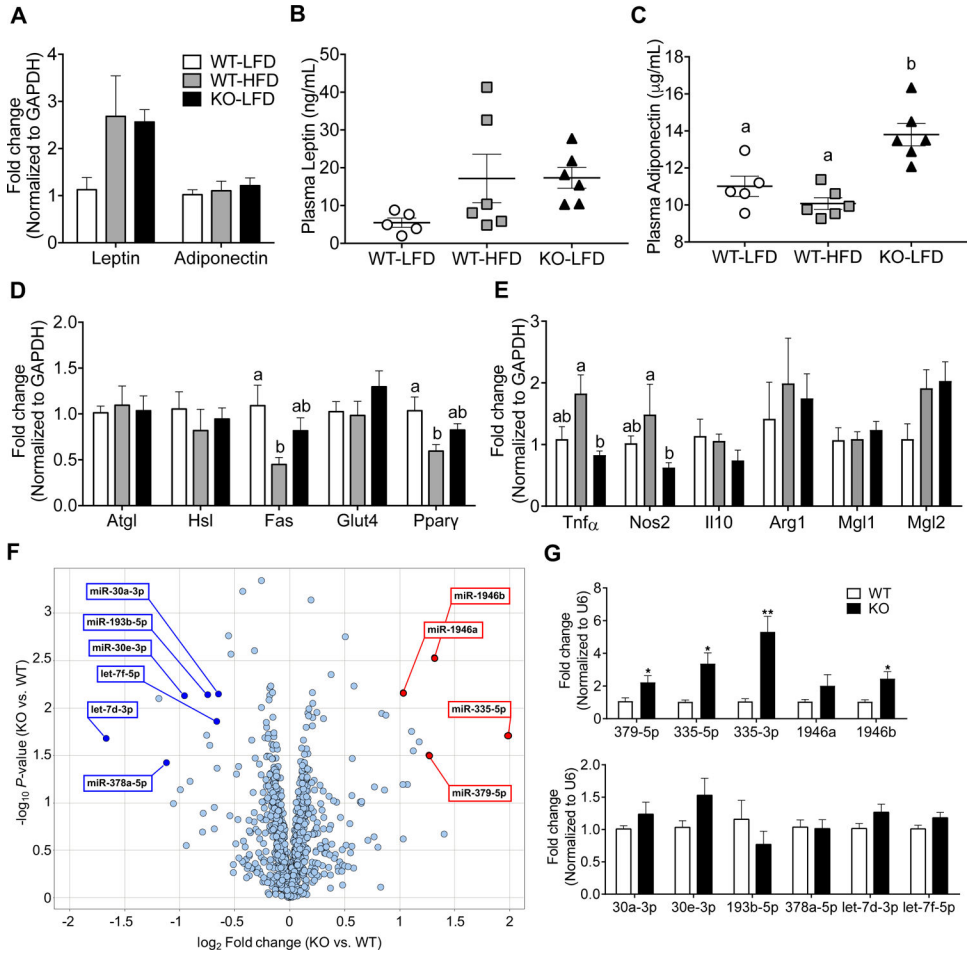

Figure 6: Biochemical profiling of epididymal white adipose tissue (eWAT).

A: Relative leptin and adiponectin mRNA levels in eWAT, *B*: Plasma leptin (in ng/mL), *C*: Plasma adiponectin (in µg/mL), one-way ANOVA ($F_{(2,14)} = 15.51$, $P = 0.0003$), *D*: Relative mRNA levels of metabolic markers - Adipose triglyceride lipase (Atgl), Hormone-sensitive lipase (Hsl), Fatty acid synthase (Fas), one-way ANOVA ($F_{(2,13)} = 3.92$, $P = 0.0466$), Insulin-regulated glucose transporter (Glut4) and Peroxisome proliferator-activated receptor gamma (Pparγ), one-way ANOVA ($F_{(2,13)} = 4.52$, $P = 0.0323$), normalized to GAPDH, in eWAT, *E*: Relative mRNA levels of inflammation markers - tumor necrosis factor (Tnf)α, one-way ANOVA ($F_{(2,13)} = 6.67$, $P = 0.0101$), nitric oxide synthase 2 (Nos2), Kruskal-Wallis test ($P = 0.0094$), interleukin-10 (Il10), arginase 1 (Arg1) and macrophage galactose-type lectin (Mgl)1 and Mgl2, normalized to GAPDH, in eWAT from adult WT and translin KO mice on a low-fat diet (LFD) as well as WT mice on a high-fat diet (HFD) for 7 weeks. For the qRT-PCR data, n = 5, 5 and 6 for the three groups, respectively. Statistical significance was assessed by one-way ANOVA or Kruskal-Wallis test followed by Bonferroni's or Dunn's post-hoc analyses, respectively. Different letters indicate statistically significant differences ($P < 0.05$); (white bars/circles = WT-LFD; grey bars/squares = WT-HFD; black bars/triangles = KO-LFD). *F:* MicroRNA expression pattern in eWAT from translin KO versus WT mice. Volcano plot showing the global microRNA changes in translin KO vs. WT eWAT. All mouse microRNAs present on the Affymetrix miRNA 4.0

array are plotted. Each circle represents one microRNA. The log2 fold change in translin KO versus wild type is represented on the x-axis. The y-axis shows the negative $\log_{10}$ of the *P*-value. Dark blue and red dots indicate microRNAs that were significantly decreased or increased respectively, by microarray in translin KO mice and were consequently assayed by qRT-PCR for validation. *G:* Validation of microarray results by qRT-PCR. n = 6/group. Data are expressed as Mean ± SEM. $*P < 0.05$, $**P < 0.01$, and $***P < 0.001$; (white bars = WT; black bars = translin KO). In addition to the microRNAs shown here, two other candidate microRNAs, miRs −6937–5p and −1931, with a $P < 0.05$ and fold-change > 2 by microarray were undetectable by qRT-PCR.